ErbB3-Dependent Motility and Intravasation in Breast Cancer Metastasis

Chengsen Xue,[1] Fubo Liang,[2] Radma Mahmood,[3] Magalis Vuolo,[3] Jeffrey Wyckoff,[1] Hong Qian,[4] Kun-Lin Tsai,[1] Mimi Kim,[4] Joseph Locker,[3] Zhong-Yin Zhang,[2] and Jeffrey E. Segall[1]

Departments of [1]Anatomy and Structural Biology, [2]Molecular Pharmacology, [3]Pathology, and [4]Epidemiology and Population Health, Albert Einstein College of Medicine, Bronx, New York

Abstract

A better understanding of how epidermal growth factor receptor family members (ErbBs) contribute to metastasis is important for evaluating ErbB-directed therapies. Activation of ErbB3/ErbB2 heterodimers can affect both proliferation and motility. We find that increasing ErbB3-dependent signaling in orthotopic injection models of breast cancer can enhance intravasation and lung metastasis with no effect on primary tumor growth or microvessel density. Enhanced metastatic ability due to increased expression of ErbB2 or ErbB3 correlated with stronger chemotaxis and invasion responses to heregulin β1. Suppression of ErbB3 expression reduced both intravasation and metastasis. A human breast cancer tumor tissue microarray showed a significant association between ErbB3 and ErbB2 expression and metastasis independent of tumor size. These results indicate that ErbB3-dependent signaling through ErbB3/ErbB2 heterodimers can contribute to metastasis through enhancing tumor cell invasion and intravasation *in vivo* and that ErbB-directed therapies may be useful for the inhibition of invasion independent of effects on tumor growth. (Cancer Res 2006; 66(3): 1418-26)

Introduction

Tumor cell metastasis is a complex process consisting of multiple steps (1). These steps include growth of the primary tumor, growth of vessels (blood vessels and lymphatics) into and around the tumor, intravasation, transport to other parts of the body, arrest, and growth at distant sites. The initial stages of primary tumor growth and angiogenesis have been well studied and are key initial steps for enabling metastasis to proceed. However, many tumors can grow to a significant size without metastasizing, and a better understanding of the factors that contribute to intravasation and metastasis is critical to developing better prognostic and therapeutic options for cancer patients.

Epidermal growth factor (EGF) receptor (EGFR) family members (ErbBs) are currently major targets of anticancer strategies (2–4) and identifying the contributions of ErbBs to tumor cell metastasis is important for the development of useful anti-ErbB therapies. The EGFR family has four members: ErbB1 (EGFR, HER-1), ErbB2 (HER-2/*neu*), ErbB3, and ErbB4 (5, 6). Twenty percent to 30% of human breast cancers have been found to overexpress ErbB2, and ErbB2 overexpression is significantly associated with decreased disease-free survival and overall survival (3, 7, 8). Normal activation of ErbB2 occurs through formation of heterodimers with other EGFR family members that can bind ligands, such as ErbB3 (9, 10). ErbB3 binds heregulin but is unable to stimulate cellular responses on its own due to a defective kinase domain. Binding of heregulin to ErbB3 can generate ErbB3/ErbB2 heterodimers, leading to activation of mitogen-activated protein kinase (MAPK), phosphatidylinositol 3-kinase (PI3K), and src (6, 11). Mutation of the ErbB3 sites coupling to these pathways reduces heregulin-induced DNA synthesis and colony formation in soft agar by NIH 3T3 cells (12). Suppression of either ErbB2 or ErbB3 function in SKBR3, MB361, or BT474 cell lines results in cell cycle arrest in G_1 (13) *in vitro. In vivo*, suppression of heregulin expression in MDA-MB-231 cells blocks tumor growth (14), and tumors induced by expression of ErbB2 in the mammary gland often show overexpression of ErbB3 (15).

Heregulin also stimulates chemotaxis and invasion mediated by ErbB3/ErbB2 heterodimers (16, 17). Activation of the PI3K and MAPK pathways can be important for cell motility and chemotaxis (18–22). The products of PI3K regulate the cytoskeleton through Rho family G proteins as well as Akt (23–25). MAPKs can regulate adhesion dynamics directly and regulate gene expression patterns important for motility and invasion (26–29). Thus, ErbB3-dependent motility responses could contribute to breast cancer metastasis independent of effects on tumor growth.

To evaluate the potential contributions of ErbB3-dependent motility responses to tumor metastasis, we evaluated the effects of overexpressing ErbBs on the metastatic properties of MDA-MB-435 (30, 31) and MTLn3 mammary tumor cells (32). We find that enhancing ErbB3/ErbB2 signaling increases intravasation and metastasis without affecting primary tumor growth. Suppression of ErbB3 expression significantly reduced intravasation and metastasis. Examination of a tumor progression microarray indicates that ErbB2 and ErbB3 expression associate positively with the presence of metastases and not with primary tumor size. We propose that ErbB3-dependent signaling can contribute to metastasis through enhancing tumor cell motility and intravasation. Our results support the development of therapies targeting cell motility to aid in the prevention and treatment of metastasis.

Materials and Methods

Cell lines. The human tumor cell line MDA-MB-435 (refs. 30, 31; American Type Culture Collection, Rockville, MD) and rat mammary MTLn3 cells (32, 33) were maintained in α-MEM (Life Technologies, Gaithersburg, MD) supplemented with 5% fetal bovine serum and penicillin/streptomycin solution (Life Technologies). The empty retroviral expression vector pLXSN and pLXSN containing the human cDNAs for ErbB1, ErbB2, ErbB3, and ErbB4 were received from David Stern (Yale University, New Haven, CT; ref. 34) and packaged in the Phoenix cell line provided by Dr. Garry P. Nolan (Stanford University, Stanford, CA; ref. 35), and cells were infected in growth medium in

Note: Supplementary data for this article are available at Cancer Research Online (http://cancerres.aacrjournals.org/).

Requests for reprints: Jeffrey E. Segall, Department of Anatomy and Structural Biology, Albert Einstein College of Medicine, 1300 Morris Park Avenue, Bronx, NY 10801. Phone: 718-430-4237; Fax: 718-430-8996; E-mail: segall@aecom.yu.edu.

doi:10.1158/0008-5472.CAN-05-0550

the presence of 4 μg/mL polybrene (Sigma, St. Louis, MO). Pools of at least 100 transductants were selected by growing in .8 mg/mL geneticin (Sigma) medium. The pools were stored as frozen stocks and used for all experiments within 10 passages. Expression of transduced ErbBs measured by fluorescence-activated cell sorting (FACS) showed no change with passage *in vitro* and after growth to form primary tumors *in vivo*.

Flow cytometric analysis. Cells ($\sim 10^6$) were incubated with specific anti-ErbB1, anti-ErbB2, anti-ErbB3, and anti-ErbB4 antibodies (NeoMarkers, Fremont, CA) for 1 hour at 4°C. After three washes in cold PBS containing 0.2% bovine serum albumin (BSA), cells were incubated with R-phycoerythrin-conjugated goat anti-mouse IgG (Jackson ImmunoResearch Laboratories, West Grove, PA) for 1 hour at 4°C. After washing, cells were suspended in PBS containing 0.2% BSA, and fluorescence was measured by flow cytometry. Cells incubated with secondary antibody only were measured at the same time to serve as background control. To semiquantitatively measure the expression level of ErbBs, standard curves were obtained by using the LinearFlow Orange Flow Cytometry Intensity Calibration kit (Molecular Probes, Eugene, OR) with the mean values of cells incubated with secondary antibody alone subtracted.

Spontaneous and experimental metastasis assays. All animal studies described here were done according to the protocols approved by the Institutional Animal Care and Use Committee of Albert Einstein College of Medicine. To measure spontaneous metastasis, the tumor cells were grown to 70% to 85% confluence before being harvested. Cells were detached by incubation in DPBS + 2 mmol/L EDTA, scraping with a rubber policeman, then centrifuged, and resuspended in DPBS at 10^7 cells/mL. MDA-MB-435 ($\sim 10^6$) or MTLn3 (5×10^5) cells were injected into the right fourth mammary fat pad from the head of 5- to 7-week-old female BALB/c severe combined immunodeficient (SCID) mice (National Cancer Institute, Bethesda, MD) in 100 μL PBS with calcium and magnesium through a 25-gauge needle. Tumor growth rate was monitored at weekly intervals by measuring in two dimensions, and tumor volumes were calculated using the formula: length × width^2 / 2. At the end point for spontaneous metastasis, mice were anesthetized with Aerrane (isoflurane, Baxter Pharmaceutical Products, Inc., Deerfield, IL). The right chest was exposed by a simple skin flap surgery. Blood was taken from the right atrium via heart puncture with a 25-gauge needle and 1 mL syringe coated with heparin and containing 0.1 mL of heparin. Blood (0.2-1.05 mL) was harvested. The blood was immediately plated into 150-mm-diameter dishes filled with 5% fetal bovine serum in α-MEM. The next day, the plates were rinsed with fresh medium and replaced with fresh medium containing 0.8 mg/mL geneticin to selectively grow tumor cells. After 4 (for MTLn3) to 10 (for MDA-MB-435) days, all colonies in the dish were counted. Tumor blood burden was calculated as total colonies in the dish divided by the volume of blood taken.

To measure experimental lung metastasis, 5×10^5 cells were injected into the lateral tail veins of 5- to 7-week-old female BALB/c SCID mice (National Cancer Institute). Eight weeks (for MDA-MB-435) or 2 weeks (for MTLn3) after injection, the mice were sacrificed, and the lungs were removed, fixed in formalin, and stained H&E sections were counted for metastasis as described below.

Tumor histology and quantitative assessment of metastasis. Samples were fixed in 10% neutral formalin buffer, embedded in paraffin, and sectioned at 5 μm and stained by H&E. For each lung sample, all micrometastases were counted at ×10 magnification and the total lung area was measured using a UMAX PowerLook III color scanner (UMAX Technologies, Inc., Dallas, TX) and Adobe Photoshop version 5.5 software. Briefly, after scanning lung sections, the cross-sectional area in pixels were measured using the luminosity window in Adobe PhotoShop. The actual lung tissue area was calculated with the formula: area (mm^2) = (number of pixels) × 0.00179. The efficiency of lung metastasis was expressed in number of metastases per square centimeter of lung area for each animal. Mean and SE were then calculated for each cell line.

Determination of blood vessel density in primary tumor. Sections (5 μm) of paraffin-embedded primary tumor samples were stained with rabbit anti-human von Willebrand factor as primary antibody (DAKO, Carpinteria, CA). Sections stained without primary antibody served as controls. DAKO peroxidase substrate kit 3,3′-diaminobenzidine (DAB) was used following the manufacturer's instructions for identifying antibody binding. Vessels were counted microscopically using a defined magnification (×200). Blood vessels in five nonoverlapping fields per tumor lesion were counted and averaged. Vascular counts included complete vessel cross-sections, partial vessel cross-sections, and small groups of positive cells. Twelve tumors from 435-PL and 10 tumors from 435-B2 were analyzed. Statistical analysis was done by unpaired *t* test.

Microchemotaxis chamber assay. A 48-well microchemotaxis chamber (Neuroprobe, Cabin John, MD) was used as described previously (36), except that L15 containing 0.35% BSA was used instead of α-MEM. For measurement of migration in response to heregulin, filters were coated with 20 μg/mL fibronectin (Sigma), whereas for measurement of responses to EGF or BTC, filters were coated with 27 μg/mL rat tail collagen (BD Biosciences, Palo Alto, CA). After inserting the filters in the chamber, 20,000 cells were plated into the wells of the upper chamber. The chambers were incubated for 4 hours at 37°C before analyzing the number of cells crossing the filter.

***In vivo* invasion assay.** Cell collection into needles placed into anesthetized animals was carried out as described previously (37, 38). In brief, 33-gauge needles are filled with Matrigel diluted 1:10 with L15-BSA, 0.01 mmol/L EDTA (pH 7.4) with or without heregulin β1 (HRGβ1). The mouse is anesthetized and laid on its back, and a small patch of skin was removed to expose the tumor. Three 25-gauge needles with inserted blocking wires are inserted into the tumor using a specially designed holder and a micromanipulator. The guide wires are then removed and the 33-gauge needles were inserted through the 25-gauge needles into the tumor. The animal is kept under anesthesia for 4 hours, after which the needles are removed, the contents were expelled onto a coverslip and stained with 4′,6-diamidino-2-phenylindole, and cells were counted.

Immunoblotting. MDA-MB-435 cells were grown to 70% confluency in a 10-cm cell culturing dish and then incubated with serum-free medium overnight. The medium was changed to fresh serum-free medium with or without 50 ng/mL HRGβ1 and cells were incubated for 0 to 15 minutes in a 5% CO_2 incubator. Cells were then washed twice with cold PBS containing 1 mmol/L vanadate and lysed in 1 mL lysis buffer [50 mmol/L Tris-HCl (pH 7.5), 1% Triton X-100, 5 mmol/L EGTA, 150 mmol/L NaCl, 10 mmol/L sodium phosphate, 10 mmol/L NaF, 1 mmol/L sodium vanadate, 1 mmol/L benzamidine, 10 μg/mL leupeptin, and 10 μg/mL aprotinin]. The plates were scraped with a rubber policeman and incubated on ice for 30 minutes. The lysate was precleared by centrifugation at 15,000 rpm for 15 minutes. Lysate protein concentration was estimated using BCA protein assay reagent (Pierce, Rockford, IL). Protein (20 μg) of each sample was loaded and separated by SDS-PAGE and transferred electrophoretically to nitrocellulose membranes, which were immunoblotted by appropriate antibodies followed by incubation with horseradish peroxidase (HRP)–conjugated secondary

Table 1. Semiquantitative measurement of expression of ErbB proteins in 435 transductants as detected by FACS analysis

Transductant	α-ErbB1 (%)	α-ErbB2 (%)	α-ErbB3 (%)	α-ErbB4 (%)
435-PL	6.2	3.9	6.6	0.04
435-B1	39.3	3.9	7.1	0.02
435-B2	5.9	39.0	5.7	0.07
435-B3	5.4	3.9	10.4	0.01
435-B4	6.2	4.5	7.0	1.1

NOTE: Data are mean fluorescence levels after subtraction of controls without primary antibody and calibrated to LinearFlow Orange Flow Cytometry beads as described in Materials and Methods where 100% corresponds to the brightest beads. MTLn3-B3 and MTLn3-PL cells had values for ErbB3 of 4.9% and 0.06%, respectively.

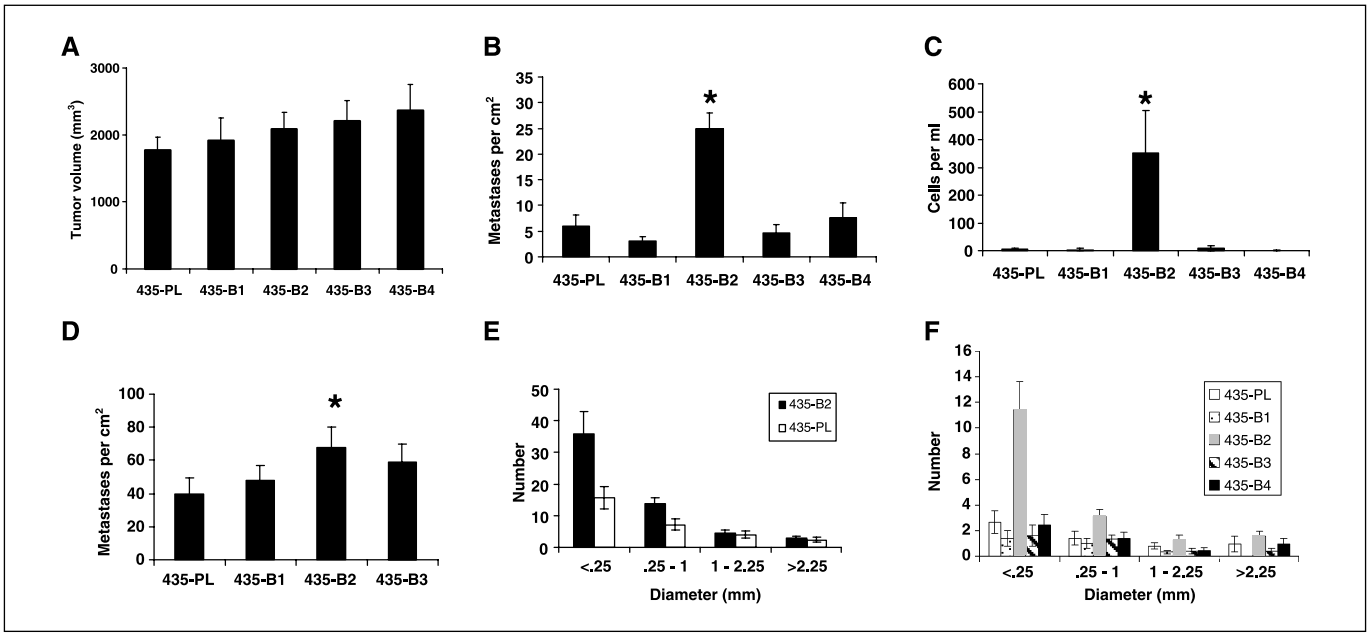

Figure 1. Increased ErbB2 expression enhances intravasation and metastasis of MDA-MB-435 Cells. *A* to *C,* cells were injected into the right mammary fat pads of SCID mice, and after 16 weeks, the animals were sacrificed and tumor volume, blood burden, and lung metastases were measured. *A,* tumor volume. *B,* density of lung metastasis. *, $P < 10^{-5}$, relative to 435-PL. *C,* blood burden (viable tumor cells/mL blood). *, $P < 0.01$ relative to 435-PL. *Columns,* mean (24 mice for 435-pLXSN, 33 mice for 435-ErbB2, and 13 mice for 435-ErbB1, 435-ErbB3, and 435-ErbB4); *bars,* SE. *D* and *E,* cells were injected into the lateral tail vein, and after 8 weeks, the mice were sacrificed and the density and diameter of lung metastases were determined. *D,* density of lung metastasis. *, $P < 0.08$, relative to 435-PL. *E,* size distribution of lung metastases in the experimental metastasis assay for 435-PL (*white columns*) and 435-B2 (*black columns*). *F,* size distribution of lung metastases in the spontaneous metastasis assay (corresponding to data in *B*) for 435-PL (*white columns*), 435-B1 (*dotted columns*), 435-B2 (*grey columns*), 435-B3 (*diagonal lines*), and 435-B4 (*black columns*). *Columns,* mean (11 mice for 435-pLXSN and 435-ErbB1, 12 mice for 435-ErbB2, and 8 mice for both 435-ErbB3 and 435-ErbB4); *bars,* SE.

antibodies. The following antibodies were used: anti-β-actin (Sigma); anti-phosphotyrosine (PY20, BD Biosciences, San Diego, CA); anti-ErbB3 monoclonal and anti-phospho-ErbB3 (Tyr^{1289}, Cell Signaling, Beverly, MA); anti-ErbB4 (Upstate, Lake Placid, NY); anti-src (Santa Cruz Biotechnology, Santa Cruz, CA); polyclonal anti–extracellular signal-regulated kinase (ERK) 1/2, anti-phospho-ERK (Thr^{202}/Tyr^{204}), anti-Akt, and anti-phospho-Akt (Ser^{473}) antibodies (Cell Signaling); anti-paxillin (Santa Cruz Biotechnology), and anti-phospho-paxillin (BioSource International, Camarillo CA). The blots were developed by the enhanced chemiluminescence (ECL) technique (ECL kit, Amersham Pharmacia Biotech) according to the manufacturer's instructions.

Immunoprecipitation. Cells were lysed in lysis buffer [50 mmol/L Tris-HCl (pH 7.5), 5 mmol/L EGTA, 1 mmol/L EDTA, 1% Triton X-100, 1 mmol/L phenylmethylsulfonyl fluoride, 2 mmol/L sodium orthovanadate, 50 mmol/L NaF, protease inhibitors]. The protein concentration was measured by BCA protein assay kit. Equal amounts of cell lysates either with or without HRGβ1 (12.5 nmol/L) treatment were incubated with anti-ErbB2 for 2 hours at 4°C followed by an incubation with protein G agarose beads (Upstate) for 1 hour. Samples were washed five times in cell lysis buffer, resuspended in 30 μL of 2× SDS sample buffer, and boiled for 5 minutes. The proteins were then resolved using a SDS-PAGE gel, transferred to a nitrocellulose membrane, and detected by Western blotting as described above.

ErbB3 RNA interference experiments. RNA interference transient transfections were done first to find the most efficient knockout sequences. Transfection-ready small interfering RNA (siRNA) duplexes against human ErbB3 were ordered from Dharmacon, Inc. (Lafayette, CO). The ErbB3 siRNA kit contains four distinct individual RNA duplexes and a mixture of siRNA duplexes (SMARTpool, Dharmacon). Cells at 60% confluency were transfected in penicillin/streptomycin-free medium with the four individual siRNA duplexes and the pooled SMARTselected siRNA by using Oligofectamine (Invitrogen, Grand Island, NY) following the manufacturer's recommended protocol. Two oligonucleotides (D-003127-05 and D-003127-07) found to suppress ErbB3 expression and inhibit responses to HRGβ1 *in vitro* were cloned into pSUPER.retro.puro (OligoEngine, Seattle, WA) as small hairpin RNAs (shRNA). A control sequence (39) that did not suppress ErbB3 expression was also cloned as a shRNA into pSUPER.retro.puro as control. Retroviruses containing the pSUPER.retro constructs were packaged using Phoenix cells. Viral supernatants were harvested, and 435-B2 and 435-PL recipient cells were infected in the presence of 4 μg/mL polybrene. After infection for 24 hours, resistant cells were selected with puromycin (3 μg/mL). FACS analysis of the stable transductants indicated that the D-003127-05 shRNA produced the strongest suppression of ErbB3 expression, and this line was used for *in vivo* studies. The sense strand sequences used for the shRNAs for the most strongly stably suppressed were GATCCCCAAGAGGATGT-CAACGGTTATTCAAGAGATAACCGTTGACATCCTCTTTTTTTA (B3 shRNA) and GATCCCCAATTCTCCGAACGTGTCACGTTTCAAGAGAACGT-GACACGTTCGGAGAATTTTTTTA (control shRNA).

Immunohistochemical staining for ErbB2 and ErbB3. Cooperative Breast Cancer Tissue Resource (CBCTR) Breast Tissue Progression microarrays were acquired from the CBCTR of the National Cancer Institute.[5] These tissue microarrays are designed by National Cancer Institute statisticians for high statistical power to detect differences in prevalence among the three stages of primary invasive ductal breast cancer: node negative, node positive, and metastatic disease. Each tissue microarray block consists of 288 0.6-mm cores representing 252 breast cancer and normal breast specimens plus replicate cores of 4 different cell lines and 4 different nonbreast tissue controls. Two sequential slices from two replicate blocks containing different cores from the same primary tumors were used to stain for ErbB2 and ErbB3.

Paraffin sections were melted at 60°C for 30 minutes, deparaffinized in xylene, rehydrated through graded alcohols to water, and washed in TBS. Slides were pretreated with 3% H_2O_2 for 10 minutes and washed in TBS. Antigen retrieval was done in a steamer for 20 minutes using 10 mmol/L sodium citrate buffer (pH 6.0). Slides were then cooled for 30 minutes at

[5] http://www-cbctr.ims.nci.nih.gov/tma.html.

room temperature. Slides were incubated in blocking solution (5% normal goat serum, 2% BSA) for 1 hour at room temperature before incubating with antibodies for 1 hour at room temperature, anti-erbB3 (Santa Cruz Biotechnology) at 1:100 or anti-ErbB2 (A0485, DAKO) at 1:250, diluted in blocking solution. Slides were then washed four times, 3 minutes each with TBS before applying biotin-labeled secondary antibody (goat anti-rabbit, DAKO) at 1:500 for 1 hour at room temperature. Slides were washed again and incubated for 30 minutes with the avidin-biotin-HRP complex as directed by DAKO. Slides were washed in TBS, and DAB was applied (DAKO) for 5 minutes (ErbB3) or 4 minutes (ErbB2) before lightly counterstaining with Harris hematoxylin (Poly Scientific, Bay Shore, NY). These concentrations and incubation times were determined to give a wide range of detections: weak positives were visible, but strong positives were not overstained. Control tests using blocking peptides (ErbB3 C-17 P, Santa Cruz Biotechnology) inhibited all ErbB3 staining.

The slides were scored independently by two pathologists, and the average scores were used for statistical analysis. Of the 192 tumors potentially available on the slides, 164 had at least one high-quality core that was successfully stained for both ErbB2 and ErbB3. The scores for these tumors were then correlated with clinical variables.

Statistics. The Wilcoxon rank sum test was used to determine two-tailed probabilities as given in the figure legends and text and to compare ErbB2 and ErbB3 expression levels between patients with metastases and patients without metastases. Multivariate analyses with metastases (yes/no) as the outcome were conducted by fitting logistic regression models. Model selection was based on backward elimination with $P < 0.10$ as the criterion for retaining covariates. The magnitude of the association between ErbB2 and ErbB3 with age and tumor size was estimated by the Spearman rank correlation coefficient. Adjustment for confounders was accomplished by fitting linear regression models to the rank transformed data. Statistical significance was defined as $P < 0.05$.

Results

Increased ErbB3-dependent signaling enhances motility, intravasation, and metastasis in MDA-MB-435 cells. To dissect the effects of increased ErbB expression on the steps of breast cancer metastasis, we used a series of retroviral vectors based on the PLXSN retrovirus (34). MDA-MB-435 cells were transduced with either empty vector (PLXSN alone) or PLXSN containing the cDNAs for ErbB1, ErbB2, ErbB3, or ErbB4 followed by selection for geneticin resistance. For each vector, several hundred resistant clones developed and were maintained as pools of resistant cells to avoid artifacts due to the use of single clones and to evaluate a range of expression levels simultaneously. Pools generated by transduction of

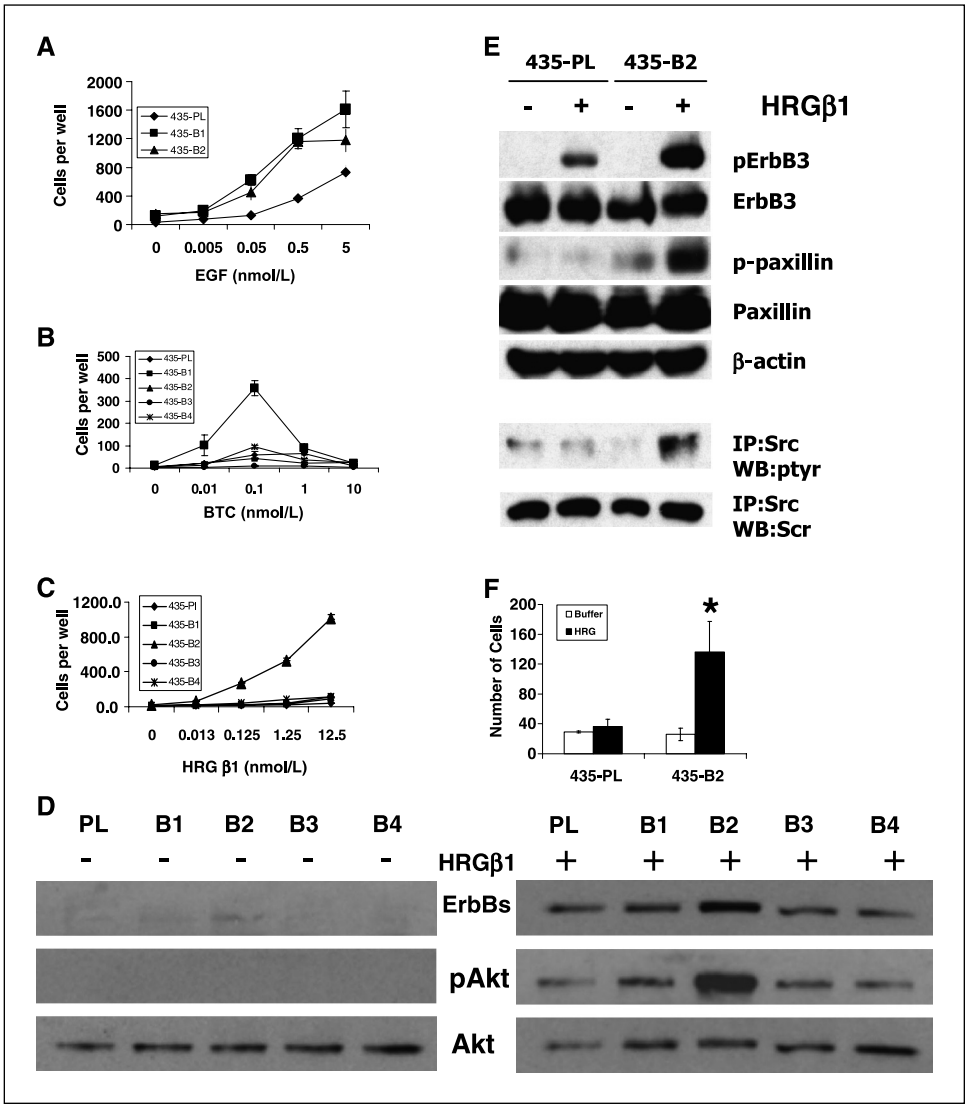

Figure 2. ErbB3-dependent chemotaxis and invasion correlates with metastasis of 435-B2 cells. Chemotactic responses to (*A*) EGF, (*B*) BTC, or (*C*) HRGβ1. *Points,* mean of at least three measurements per data point for 435-PL (♦), 435-B1 (■), 435-B2 (▲), 435-B3 (●), and 435-B4 (▨); *bars,* SE. *D,* serum-starved cells before and after exposure to HRGβ1 (12.5 nmol/L) for 15 minutes were lysed and Western blotted for phosphotyrosine (180-kDa region corresponding to ErbBs), phospho-Akt (*pAkt*), and total Akt. *E,* serum-starved cells before and after exposure to HRGβ1 (12.5 nmol/L) for 4 minutes were lysed and Western blotted directly (*top*) or the lysates were used for src immunoprecipitations (*bottom*). Phospho-ErbB3 (*pErbB3*) and phospho-paxillin (*p-paxillin*) blots used antibodies specific for phosphotyrosine at residue 1,289 for ErbB3 and residue 118 for paxillin. *F, in vivo* invasion of 435-PL and 435-B2 cells was measured in response to buffer (*white columns*; $n = 3$ needles) or HRGβ1 (*black columns*; $n = 5$ needles). *Columns,* mean of the number of cells entering the needle for each condition; *bars,* SE. *, $P < 0.05$ relative to 435-PL.

MDA-MB-435 cells with PLXSN, ErbB1, ErbB2, ErbB3, or ErbB4 retrovirus will be called 435-PL, 435-B1, 435-B2, 435-B3, or 435-B4, respectively. FACS analysis of all the lines (Table 1) indicated that each vector increased expression of the targeted ErbB compared with the 435-PL cells, and the altered expression remained constant after passage *in vitro* and *in vivo*.

We then evaluated metastasis *in vivo* using the spontaneous metastasis assay (40). We injected each of the lines into the mammary fat pads of SCID mice and measured primary tumor size, tumor cells in the blood, and lung metastases 15 to 16 weeks after injection. Tumor growth and final tumor size at analysis showed no significant differences in primary tumor growth between the various transfectants and 435-PL (Fig. 1*A*), consistent with similar growth rates observed for the lines in tissue culture (data not shown). The number of lung metastases was significantly increased only in animals carrying 435-B2 tumors (Fig. 1*B*). We have developed previously a method to measure the intravasation efficiency of primary tumors by culturing blood from the right atrium of the heart and using the number of tumor cell colonies that form to determine the number of viable tumor cells (40). This intravasation measurement showed a significant increase for animals carrying 435-B2 tumors (Fig. 1*C*). To evaluate the relative abilities of the lines to arrest and proliferate in the lungs independent of primary tumor formation and intravasation, we did an experimental metastasis assay. Cells were injected into the lateral tail veins of SCID mice, and 8 weeks later, the mice were sacrificed and the density of lung metastases was determined (Fig. 1*D*). 435-B2 cells showed a slight increase in experimental metastasis, consistent with a previous study (22).

These results suggest that for MDA-MB-435 cells increased levels of ErbB2 have a major effect on intravasation, a minor effect on later stages of metastasis at the target organ (as assayed by experimental metastasis), and little effect on proliferation. The distributions of lung metastasis sizes for both experimental (Fig. 1*E*) and spontaneous metastasis (Fig. 1*F*) assays show the largest increase in the number of small metastases rather than the number of large metastases, consistent with ErbB2 enhancing steps early in the metastasis process as opposed to enhancing the growth rate of established metastases.

To test whether the increased intravasation might be due to increased angiogenesis, we evaluated microvessel density as detected by immunostaining for von Willebrand factor. There was no significant difference (21 ± 4 for 435-PL versus 28 ± 5 for 435-B2; $P < 0.22$); thus, changes in angiogenesis are unlikely to explain the increased intravasation observed for 435-B2 tumors. Examination of overall tumor structure by H&E staining also did not show dramatic differences between tumors from any of the cell lines.

Because proliferation and angiogenesis were not enhanced in 435-B2 cells, it is possible that the increased intravasation reflects increased motility or chemotaxis. To determine whether chemotactic response to a particular heterodimer pair formed by ErbB2 was correlated with enhanced intravasation and metastasis, we evaluated responses to EGF, HRGβ1, and BTC (17). EGF responses are mediated by ErbB1, HRGβ1 responses are mediated by ErbB3 and ErbB4, and BTC responses are mediated by ErbB1 and ErbB4 (5). Both 435-B1 and 435-B2 lines showed increased chemotactic responses to EGF (Fig. 2*A*), arguing against responses to EGF via ErbB1 homodimers or ErbB1/ErbB2 heterodimers being responsible for the increased metastatic capabilities of the 435-B2 line (because 435-ErbB1 tumors do not show increased metastasis). Chemotactic responses to BTC were increased in the 435-B1 and 435-B4 lines (Fig. 2*B*) but not in 435-B2, arguing against

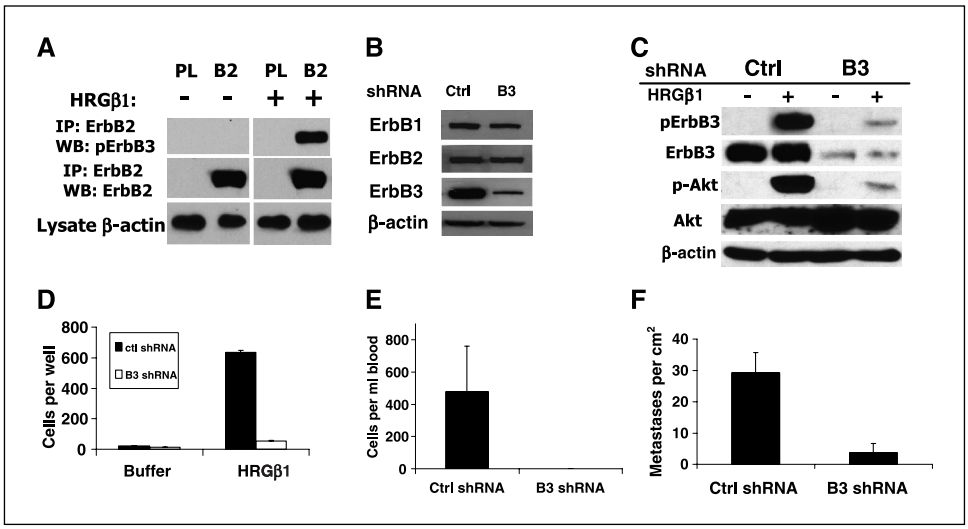

Figure 3. ErbB3/ErbB2 heterodimers mediate HRGβ1-induced signaling, migration, and metastasis. *A,* ErbB3/ErbB2 heterodimers form on HRGβ1 stimulation in 435-B2 cells. ErbB2 was immunoprecipitated from cell lysates before or 4 minutes after stimulation with 12.5 nmol/L HRGβ1 and the immunoprecipitates were blotted for total ErbB2 and phospho-ErbB3 (Tyr^{1289}). On longer exposure, a low level of immunoprecipitated ErbB2 from 435-PL cells is detectable, consistent with their low levels of ErbB2. Total cell lysate β-actin is also shown. *B,* Western blot analysis of ErbB1, ErbB2, and ErbB3 expression in stable lines transduced by pSUPER.retro containing control shRNA (*Ctrl*) or ErbB3-targeted shRNA (*B3*). Scanning and quantitation of the bands indicated changes of <10% for ErbB1 and ErbB2 and >80% for ErbB3. ErbB4 expression was undetectable in either line by Western blot. *C,* suppression of ErbB3 expression in 435-B2 cells inhibits HRGβ1-induced ErbB3 phosphorylation and Akt activation. Cells were stimulated with 12.5 nmol/L HRGβ1 for 4 minutes and lysed, and Western blots of the lysates were evaluated for phosphorylation of ErbB3 and Akt. *D,* suppression of ErbB3 expression inhibits chemotaxis to HRGβ1 in 435-PL and 435-B2 cells. 435-B2 cells stably transduced by pSUPER.retro driving expression of either control shRNA (*black columns*) or B3 shRNA (*white columns*) were incubated with buffer or 12.5 nmol/L HRGβ1 in the lower chamber. *Columns,* mean of 11 measurements per condition; *bars,* SE. *E* and *F,* spontaneous lung metastasis analysis. 435-B2 cells transduced with pSUPER.retro driving expression of either control shRNA (11 animals) or ErbB3-targeted shRNA (13 animals) were injected into the mammary fat pads of SCID mice. Primary tumor growth was followed and animals were sacrificed for the measurement of blood burden (*E*; $P < 0.02$) and lung metastasis (*F*; $P < 0.001$) once the average tumor size was >2,000 mm^3 (127 days for control shRNA tumors and 148 days for B3 shRNA tumors). *Columns,* mean; *bars,* SE.

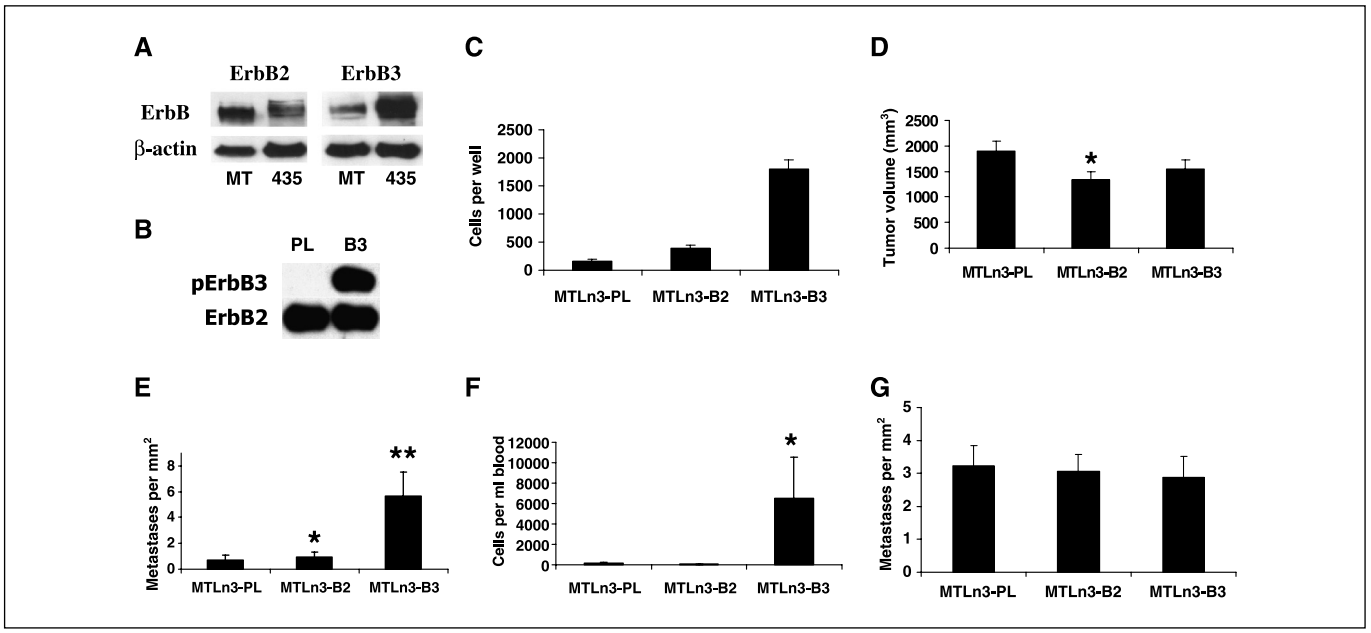

Figure 4. Increasing ErbB3 expression in MTLn3 cells strongly enhances HRGβ1 chemotaxis, intravasation, and metastasis. *A,* Western blot of ErbB2 and ErbB3 expression in MTLn3-PL (*MT*) and 435-PL (*435*) lines. *B,* MTLn3-B3 cells show enhanced ErbB3/ErbB2 heterodimer formation on HRGβ1 stimulation. Cells were stimulated with 12.5 nmol/L HRGβ1 for 1 minute, lysates were made, ErbB2 was immunoprecipitated, and immunoprecipitates were Western blotted for phospho-ErbB3 (Tyr^{1289}; *pErbB3*) or ErbB2. *C,* chemotaxis to 12.5 nmol/L HRGβ1 using a 48-well microchemotaxis chamber. *D* to *F,* for determination of spontaneous metastatic properties, MTLn3-PL (25 mice), MTLn3-B2 (15 mice), or MTLn3-B3 (22 mice) cells were injected into the right mammary fat pads of SCID mice. After 5 weeks, the animals were sacrificed and tumor volume (*D*; *, $P < 0.05$), lung metastases (*E*; *, $P < 0.05$; **, $P < 0.002$), and blood burden (*F*; *, $P < 0.001$) were measured as described in Materials and Methods. *G,* for determination of experimental metastatic properties, cells were injected into the lateral tail vein (10 mice per cell line). After 2 weeks, the mice were sacrificed and the density of lung metastases was determined. *Columns,* mean; *bars,* SE.

ErbB4-ErbB2 heterodimer or ErbB4 homodimer signaling being important for the increased metastasis of the 435-B2 line.

Chemotactic responses to HRGβ1 were only increased in the 435-B2 line (Fig. 2*C*), correlating with the increased metastatic properties of this line. Similarly, HRGβ1 stimulated tyrosine phosphorylation of ErbBs and Akt activation to the greatest extent in 435-B2 cells (Fig. 2*D*). HRGβ1 stimulation increased tyrosine phosphorylation of ErbB3, paxillin, and src in 435-B2 cells compared with the 435-PL control (Fig. 2*E*). We did not see increased ERK activation (data not shown). Thus, in tissue culture, 435-B2 cells showed the strongest signal transduction and chemotaxis responses to HRGβ1. To test whether increased HRGβ1 1 could also stimulate increased invasive responses *in vivo*, we did an *in vivo* invasion assay (41). In this assay, microneedles containing Matrigel alone or Matrigel with HRGβ1 are inserted into tumors in anesthetized animals for 3 hours. The needles are then removed and the numbers of cells that invade into the microneedles are counted. The 435-B2 tumors showed significantly enhanced invasion in response to HRGβ1 (Fig. 2*F*) compared with 435-PL tumors. Invasion into needles containing Matrigel alone was the same for 435-PL and 435-B2 tumors.

The above results argue for an ErbB3/ErbB2 heterodimer being important for enhanced intravasation and metastasis in the 435-B2 cells. To determine if there were greater levels of an active ErbB3/ErbB2 heterodimer in 435-B2 cells after HRGβ1 stimulation, we immunoprecipitated ErbB2 and blotted the immunoprecipitates using an antibody specific for ErbB3 phosphorylation at Tyr^{1289} (Fig. 3*A*). In 435-B2 cells, we found a strong association of ErbB2 with phospho-ErbB3 after HRGβ1 stimulation, consistent with increased heterodimer formation in 435-B2 cells. To directly test whether ErbB3 is required for HRGβ1 responses and metastasis in 435-B2 cells, we reduced ErbB3 levels using siRNA. Sequences from the Dharmacon SMARTpool collection specific for ErbB3 were tested and cloned as shRNAs into pSUPER.retro as well as a control sequence that did not alter ErbB3 expression. Retroviruses were generated and used to transduce the 435-B2 line, and the shRNA most effective at stably suppressing ErbB3 expression was studied further. ErbB1 and ErbB2 expression was altered by <10%, whereas ErbB3 expression was reduced by >80% (Fig. 3*B*). ErbB3 suppression reduced ErbB3 tyrosine phosphorylation and Akt activation induced by HRGβ1 (Fig. 3*C*) and reduced HRGβ1 chemotaxis by 90% (Fig. 3*D*). This confirms that the enhanced signaling and chemotaxis in response to HRGβ1 in 435-B2 cells is mediated by an ErbB3/ErbB2 heterodimer. *In vivo*, suppression of ErbB3 delayed tumor growth, but at equivalent tumor sizes, both intravasation (Fig. 3*E*) and metastasis (Fig. 3*F*) were strongly reduced for 435-B2 tumors expressing ErbB3 shRNA compared with tumors expressing control shRNA. Thus, ErbB3 is critical for the high rates of intravasation and metastasis exhibited by 435-B2 cells.

Increasing ErbB3 expression in the context of high ErbB2 can enhance metastasis. To determine whether ErbB3/ErbB2 heterodimers could enhance intravasation and metastasis in other breast cancer lines, we examined MTLn3 rat mammary adenocarcinoma cells. As shown in Fig. 4*A*, MTLn3 cells show higher levels of ErbB2 expression and lower levels of ErbB3 expression than MDA-MB-435 cells. MTLn3 cells were transduced with pLXSN-derived retroviruses driving expression of ErbB3 and ErbB2 or lacking an insert and are designated as MTLn3-B3, MTLn3-B2, or MTLn3-PL, respectively. The expression of ErbB proteins was confirmed by flow cytometry and Western blot. MTLn3-B3 showed increased formation of an active ErbB3/ErbB2 heterodimer with HRGβ1 stimulation

as evidenced by blotting ErbB2 immunoprecipitates with an antibody against phospho-ErbB3 (Fig. 4*B*). Chemotaxis to HRGβ1 was slightly increased in MTLn3-B2 cells and most strongly enhanced in MTLn3-B3 cells (Fig. 4*C*), with no effect on growth rate *in vitro*.

The metastatic properties of these lines were then measured using the spontaneous and experimental metastasis assays. Primary tumor growth rate was slightly reduced for both MTLn3-B2 and MTLn3-B3 compared with the control MTLn3-PL line (Fig. 4*D*). On the other hand, lung metastasis was slightly increased in the MTLn3-B2 line and strongly increased in the MTLn3-B3 line (Fig. 4*E*). In parallel with the increased lung metastasis, MTLn3-B3 generated tumors had significantly increased intravasation (Fig. 4*F*). Lung colonization efficiency as determined by the experimental metastasis assay showed no differences among the MTLn3-B3, MTLn-B2, and MTLn3-PL lines (Fig. 4*G*). Thus, in the context of high levels of ErbB2, increased expression of ErbB3 also can enhance chemotaxis, intravasation, and metastasis independent of effects on primary tumor growth.

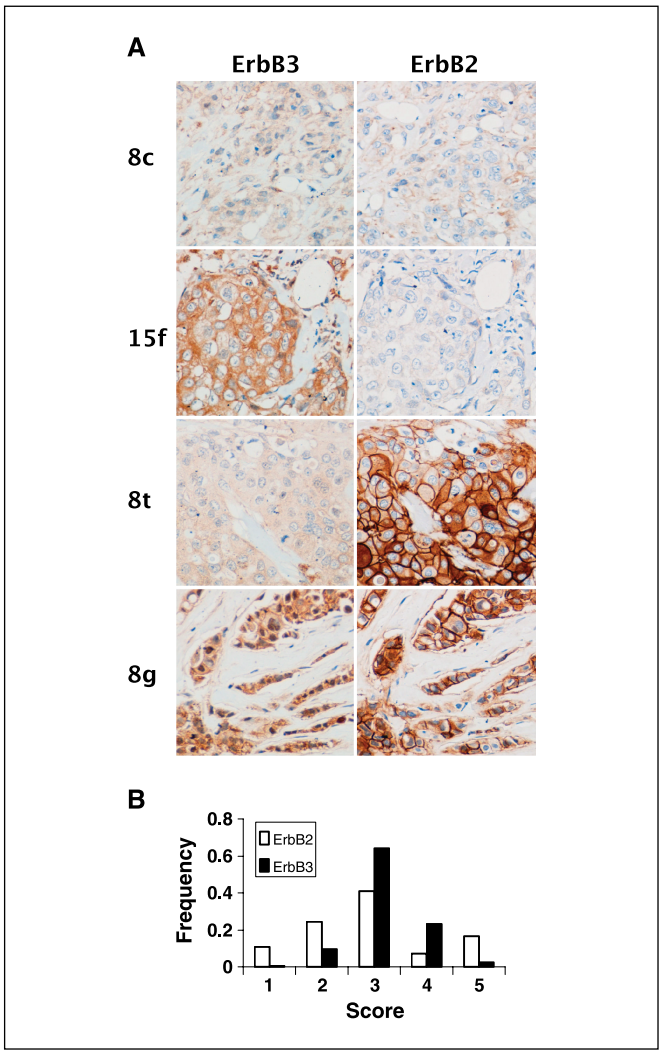

Figure 5. Tumor tissue microarray analysis of ErbB2 and ErbB3 expression. *A,* four representative tumors showing the range of ErbB3 and ErbB2 staining combinations identified by their locations in the tissue microarray. *B,* distribution of staining intensities for ErbB2 (*white columns*) and ErbB3 (*black columns*) for the tumor tissue microarray.

Increased expression of ErbB2 and ErbB3 correlates with increased human breast cancer metastasis. The results in the previous sections suggest that higher levels of ErbB2 and ErbB3 in combination could enhance tumor cell metastasis independent of primary tumor growth in human breast cancer. To test this hypothesis, we made use of a breast cancer progression microarray provided by the CBCTR, a resource supported by the National Cancer Institute. The microarray contains cores from 192 invasive human primary breast cancers. Clinical data for the tumors includes patient age, race, primary tumor size, estrogen receptor (ER), progesterone receptor (PR), positive lymph nodes, and distant metastasis. We stained the tissue microarrays in duplicate for ErbB2 and ErbB3.

ErbB2 staining tended to be membrane associated, whereas ErbB3 staining was more cytoplasmic, with some membrane association present (Fig. 5*A*). The stain intensity and localization was graded independently by two pathologists on a 0 (no staining) to 5 (maximum staining) scale. Overall staining intensity scores by the two pathologists were well correlated, whereas membrane staining scores were not; therefore, overall staining was used for statistical analysis.

A total of 164 cores contained adequately stained tumor samples for both ErbB2 and ErbB3 staining and were used for statistical analysis. The distributions of staining intensity for ErbB2 and ErbB3 are shown in Fig. 5*B*. ErbB2 staining showed a broad range, with a subset of intensely staining tumors, as has been well established. ErbB3 staining had a narrower range, with very few weakly staining tumors. ErbB3 staining showed a modest but significant correlation with ErbB2 staining (Spearman ρ coefficient = 0.31; $P < 0.0001$).

The bivariate and multivariate associations of ErbB2 and ErbB3 staining scores with the following clinical variables were evaluated: tumor size, nodal status, number of nodes, ER status, PR status, grade, and metastases. The staining intensities for ErbB2 and ErbB3 were significantly elevated in patients with metastases compared with patients without metastases ($P = 0.02$ for both ErbB and ErbB3). Interestingly, a significantly greater association with metastasis was seen for the sum: ErbB2 + ErbB3 ($P = 0.005$), indicating that both ErbB2 and ErbB3 provide information regarding the metastatic capability of the primary tumor, consistent with the predictions from our animal model studies. ErbB2 and ErbB3 were also positively associated with metastases in multivariate analyses ($P = 0.0083$ and 0.017, respectively) after adjusting for tumor size and ER status, the only confounders that were retained in the final logistic regression models. We also evaluated the sum (ErbB2 + ErbB3) in the multivariate model, and the predictive value of the sum was again more highly significant than either one individually ($P = 0.0027$), consistent with both ErbB2 and ErbB3 independently providing information regarding the metastatic capability of the primary tumor. On segregating the data into groups corresponding to high, intermediate, and low ErbB2 (Supplementary Table S1), we found that the presence of metastases was most significantly correlated with ErbB3 expression in tumors with intermediate levels of ErbB2. A possible interpretation of this result is that, at low levels of ErbB2, ErbB3 is unable to signal (consistent with its limited kinase activity), whereas high levels of ErbB2 may produce autoactivation of ErbB2 that does not require interaction with ErbB3.

The associations of ErbB2 and ErbB3 with ER status, PR status, grade, node status, and number of nodes were not significant. ErbB3 staining correlated positively with age ($\rho = 0.20$; $P = 0.009$)

and negatively with tumor size ($\rho = -0.16$; $P < 0.041$), but these associations did not retain significance in multivariate regression analyses. ErbB2 was not significantly associated with other clinical variables.

Discussion

In the studies reported here, we provide the first direct evidence that ErbB3-dependent signaling can contribute to metastasis of breast cancer through enhancing intravasation. Because tumor formation and angiogenesis were not increased in parallel with intravasation and metastasis, it is unlikely that the proliferative consequences of ErbB3 signaling are the basis for the enhanced metastasis we observed. Our results support a model (13, 22, 42) in which both biological effects of ErbB3 signaling (enhanced tumorigenesis and invasion) can contribute to breast cancer. In this model, low levels of ErbB3 signaling are sufficient for tumorigenesis, forming an oncogenic unit (13) through generation of signals that suppress apoptosis and enhance cell cycle progression. Because ErbB3 signaling occurs mainly through heterodimerization with ErbB2, low levels of signaling could occur in tumors expressing high levels of either ErbB2 or ErbB3 through spontaneous heterodimer formation (in the absence of heregulin) or in tumors expressing lower levels of ErbB3/ErbB2 that are exposed to heregulin. However, chemotaxis and invasion would be relatively weak, and such tumors would be unable to effectively use ErbB3/ErbB2 signaling for invasion. On the other hand, tumors expressing moderate to high levels of both ErbB2 and ErbB3 (potentially through genomic amplification) could show strong chemotaxis and invasion, resulting in enhanced intravasation and metastasis due to ErbB3/ErbB2 signaling.

In this model, the endogenous ErbB2 and ErbB3 levels in the MDA-MB-435 and MTLn3 cells are sufficient for full stimulation of tumorigenesis *in vivo* but are suboptimal for maximal chemotaxis and invasion [low levels of ErbB2 in MDA-MB-435 cells (16, 22, 43) and low levels of ErbB3 in MTLn3 cells]. Overexpressing the limiting partner (ErbB2 in MDA-MB-435 cells or ErbB3 in MTLn3 cells) enables stronger signaling resulting in enhanced chemotaxis and invasion without affecting primary tumor growth. The enhanced chemotaxis and invasion could reflect both immediate ErbB activation (17) and ErbB-induced alterations in gene expression patterns (44, 45). Suppression of ErbB3 in 435-B2 cells reduces the signaling efficiency below that which is optimal for tumorigenesis, resulting in slowed tumor growth. However, even on growth of the tumors to a large size, intravasation and metastasis remain reduced as predicted if an ErbB3-dependent intravasation step is required for efficient metastasis of the 435-B2 cells.

The tumor tissue microarray analysis of human breast cancer expression of ErbB3 and ErbB2 is consistent with this model in two ways. First, the combination of ErbB2 and ErbB3 was more significantly associated with the presence of metastasis than the level of ErbB2 or ErbB3 staining alone, consistent with the importance of a complex of ErbB2 and ErbB3 for invasion and metastasis. Second, there was no correlation between tumor size and the combination of ErbB2 and ErbB3, suggesting that these tumors have progressed past the early steps in tumorigenesis. In addition, ErbB3 expression levels may be useful in prognosis of metastasis for tumors that have intermediate levels of ErbB2.

This model has implications for therapies that are targeted to inhibition of ErbB2 or ErbB3 (and by extension other receptors that have functions in both growth control and chemotaxis). It suggests that, for the subset of tumors in which ErbB3/ErbB2 signaling is near the threshold required for tumorigenesis, partial suppression of either ErbB2 or ErbB3 could directly affect tumor growth as is seen for a limited number of tumors. However, for the subset of tumors that have moderate to high levels of both ErbB2 and ErbB3, partial suppression might only affect chemotaxis and invasion without affecting tumor growth, similar in action to metastasis suppressors (46). Such tumors would be scored as nonresponding in terms of growth but might still be inhibited in terms of invasion. Our results support the targeting of ErbB3-dependent signaling for inhibition of invasion in tumors overexpressing ErbB2 and ErbB3. Suppression of invasion would contribute to limiting the further spread of tumor fragments and metastases that remain after removal of the primary tumor and could be useful in combination with treatments that directly target growth (47). In addition, patients with tumors having high levels of ErbB3 in the presence of intermediate to high levels of ErbB2 are at higher risk of metastasis and thus might need to be more aggressively treated.

Acknowledgments

Received 2/17/2005; revised 10/11/2005; accepted 11/18/2005.

Grant support: CA77522 and CA100324 (J.E. Segall) and CA69202 (Z-Y. Zhang) for support.

The costs of publication of this article were defrayed in part by the payment of page charges. This article must therefore be hereby marked *advertisement* in accordance with 18 U.S.C. Section 1734 solely to indicate this fact.

We thank the members of the Cox, Segall, and Condeelis laboratories and Glenn Kroog for comments and suggestions and David Stern, Bristol Myers Squibb, and Gary P. Nolan for generously providing the reagents.

References

1. Chambers AF, Groom AC, MacDonald IC. Metastasis: dissemination and growth of cancer cells in metastatic sites. Nat Rev Cancer 2002;2:563–72.
2. Shawver LK, Slamon D, Ullrich A. Smart drugs: tyrosine kinase inhibitors in cancer therapy. Cancer Cell 2002;1:117–23.
3. McKeage K, Perry CM. Trastuzumab: a review of its use in the treatment of metastatic breast cancer overexpressing HER2. Drugs 2002;62:209–43.
4. Mendelsohn J, Baselga J. Status of epidermal growth factor receptor antagonists in the biology and treatment of cancer. J Clin Oncol 2003;21:2787–99.
5. Yarden Y, Sliwkowski MX. Untangling the ErbB signalling network. Nat Rev Mol Cell Biol 2001;2:127–37.
6. Holbro T, Civenni G, Hynes NE. The ErbB receptors and their role in cancer progression. Exp Cell Res 2003;284:99–110.
7. Slamon DJ, Clark GM, Wong SG, et al. Human breast cancer: correlation of relapse and survival with amplification of the HER-2/*neu* oncogene. Science 1987;235:177–82.
8. Press MF, Pike MC, Chazin VR, et al. Her-2/*neu* expression in node-negative breast cancer: direct tissue quantitation by computerized image analysis and association of overexpression with increased risk of recurrent disease. Cancer Res 1993;53:4960–70.
9. Stern DF. ErbBs in mammary development. Exp Cell Res 2003;284:89–98.
10. Citri A, Skaria KB, Yarden Y. The deaf and the dumb: the biology of ErbB-2 and ErbB-3. Exp Cell Res 2003;284:54–65.
11. Alimandi M, Romano A, Curia MC, et al. Cooperative signaling of ErbB3 and ErbB2 in neoplastic transformation and human mammary carcinomas. Oncogene 1995;10:1813–21.
12. Vijapurkar U, Kim MS, Koland JG. Roles of mitogen-activated protein kinase and phosphoinositide 3′-kinase in ErbB2/ErbB3 coreceptor-mediated heregulin signaling. Exp Cell Res 2003;284:291–302.
13. Holbro T, Beerli RR, Maurer F, et al. The ErbB2/ErbB3 heterodimer functions as an oncogenic unit: ErbB2 requires ErbB3 to drive breast tumor cell proliferation. Proc Natl Acad Sci U S A 2003;100:8933–8.
14. Tsai MS, Shamon-Taylor LA, Mehmi I, Tang CK, Lupu R. Blockage of heregulin expression inhibits tumorigenicity and metastasis of breast cancer. Oncogene 2003;22:761–8.
15. Siegel PM, Ryan ED, Cardiff RD, Muller WJ. Elevated expression of activated forms of Neu/ErbB-2 and ErbB-3 are involved in the induction of mammary tumors in

transgenic mice: implications for human breast cancer. EMBO J 1999;18:2149–64.
16. Adelsman MA, McCarthy JB, Shimizu Y. Stimulation of β1-integrin function by epidermal growth factor and heregulin-β has distinct requirements for erbB2 but a similar dependence on phosphoinositide 3-OH kinase. Mol Biol Cell 1999;10:2861–78.
17. Spencer KS, Graus-Porta D, Leng J, Hynes NE, Klemke RL. ErbB2 is necessary for induction of carcinoma cell invasion by ErbB family receptor tyrosine kinases. J Cell Biol 2000;148:385–97.
18. Hinton DR, He S, Graf K, et al. Mitogen-activated protein kinase activation mediates PDGF-directed migration of RPE cells. Exp Cell Res 1998;239:11–5.
19. Summy M, Gallick GE. Src family kinases in tumor progression and metastasis. Cancer Metastasis Rev 2003; 22:337–58.
20. Chausovsky A, Waterman H, Elbaum M, Yarden Y. Molecular requirements for the effect of neuregulin on cell spreading, motility and colony organization. Oncogene 2000;19:878–88.
21. Adam L, Vadlamudi R, Kondapaka SB, et al. Heregulin regulates cytoskeletal reorganization and cell migration through the p21-activated kinase-1 via phosphatidylinositol-3 kinase. J Biol Chem 1998;273: 28238–46.
22. Tan T, Yao J, Yu D. Overexpression of the c-erbB-2 gene enhanced intrinsic metastasis potential in human breast cancer cells without increasing their transformation abilities. Cancer Res 1997;57:1199–205.
23. Katso R, Okkenhaug K, Ahmadi K, et al. Cellular function of phosphoinositide 3-kinases: implications for development, homeostasis, and cancer. Annu Rev Cell Dev Biol 2001;17:615–75.
24. Fukata M, Nakagawa M, Kaibuchi K. Roles of Rho-family GTPases in cell polarisation and directional migration. Curr Opin Cell Biol 2003;15:590–7.
25. Merlot S, Firtel RA. Leading the way: directional sensing through phosphatidylinositol 3-kinase and other signaling pathways. J Cell Sci 2003;116:3471–8.
26. Reddy KB, Nabha SM, Atanaskova N. Role of MAP kinase in tumor progression and invasion. Cancer Metastasis Rev 2003;22:395–403.
27. Xia Y, Karin M. The control of cell motility and epithelial morphogenesis by Jun kinases. Trends Cell Biol 2004;14:94–101.
28. Webb DJ, Donais K, Whitmore LA, et al. FAK-Src signalling through paxillin, ERK and MLCK regulates adhesion disassembly. Nat Cell Biol 2004;6:154–61.
29. Ozanne BW, McGarry L, Spence HJ, et al. Transcriptional regulation of cell invasion: AP-1 regulation of a multigenic invasion programme. Eur J Cancer 2000;36: 1640–8.
30. Price JE. Analyzing the metastatic phenotype. J Cell Biochem 1994;56:16–22.
31. Sellappan S, Grijalva R, Zhou X, et al. Lineage infidelity of MDA-MB-435 cells: expression of melanocyte proteins in a breast cancer cell line. Cancer Res 2004;64:3479–85.
32. Lichtner RB, Nicolson GL. Organization of cytoskeletal structures in 13762NF rat mammary adenocarcinoma cell lines and clones of different metastatic potentials. Invasion Metastasis 1987;7:73–82.
33. Welch DR, Neri A, Nicolson GL. Comparison of "spontaneous" and "experimental" metastasis using rat 13762 mammary adenocarcinoma metastatic cell clones. Invasion Metastasis 1983;3:65–80.
34. Riese DJ, van Raaij TM, Plowman GD, Andrews GC, Stern DF. The cellular response to neuregulins is governed by complex interactions of the erbB receptor family. Mol Cell Biol 1995;15:5770–6.
35. Pear WS, Nolan GP, Scott ML, Baltimore D. Production of high-titer helper-free retroviruses by transient transfection. Proc Natl Acad Sci U S A 1993;90:8392–6.
36. Wyckoff JB, Insel L, Khazaie K, et al. Suppression of ruffling by EGF in chemotactic cells. Exp Cell Res 1998; 242:100–9.
37. Wyckoff J, Wang W, Lin EY, et al. A paracrine loop between tumor cells and macrophages is required for tumor cell migration in mammary tumors. Cancer Res 2004;64:7022–9.
38. Wang W, Wyckoff JB, Wang Y, et al. Gene expression analysis on small numbers of invasive cells collected by chemotaxis from primary mammary tumors of the mouse. BMC Biotechnol 2003;3:13.
39. Kempiak SJ, Yip SC, Backer JM, Segall JE. Local signaling by the EGF receptor. J Cell Biol 2003;162:781–7.
40. Wyckoff JB, Jones JG, Condeelis JS, Segall JE. A critical step in metastasis: *in vivo* analysis of intravasation at the primary tumor. Cancer Res 2000;60:2504–11.
41. Wyckoff JB, Segall JE, Condeelis JS. The collection of the motile population of cells from a living tumor. Cancer Res 2000;60:5401–4.
42. Xu FJ, Stack S, Boyer C, et al. Heregulin and agonistic anti-p185(c-erbB2) antibodies inhibit proliferation but increase invasiveness of breast cancer cells that overexpress p185(c-erbB2): increased invasiveness may contribute to poor prognosis. Clin Cancer Res 1997;3:1629–34.
43. Aguilar Z, Akita RW, Finn RS, et al. Biologic effects of heregulin/*neu* differentiation factor on normal and malignant human breast and ovarian epithelial cells. Oncogene 1999;18:6050–62.
44. Yao J, Xiong S, Klos K, et al. Multiple signaling pathways involved in activation of matrix metalloproteinase-9 (MMP-9) by heregulin-β1 in human breast cancer cells. Oncogene 2001;20:8066–74.
45. Grothey A, Hashizume R, Ji H, et al. C-erbB-2/HER-2 upregulates fascin, an actin-bundling protein associated with cell motility, in human breast cancer cell lines. Oncogene 2000;19:4864–75.
46. Shevde LA, Welch DR. Metastasis suppressor pathways—an evolving paradigm. Cancer Lett 2003;30:1–20.
47. Sledge GW, Jr., Miller KD. Exploiting the hallmarks of cancer: the future conquest of breast cancer. Eur J Cancer 2003;39:1668–75.

ErbB3-Dependent Motility and Intravasation in Breast Cancer Metastasis

Chengsen Xue, Fubo Liang, Radma Mahmood, et al.

Cancer Res 2006;66:1418-1426.